

## Precise density-functional method for periodic structures

G. te Velde\* and E. J. Baerends†

*Afdeling Theoretische Chemie, Scheikundig Laboratorium der Vrije Universiteit,  
De Boelelaan 1083, 1081 HV Amsterdam, The Netherlands*

(Received 29 October 1990; revised manuscript received 3 May 1991)

A density-functional method for calculations on periodic systems (periodicity in one, two, or three dimensions) is presented in which all aspects of numerical precision are efficiently controlled. Highly accurate and rapidly converging strategies have been implemented for (a) the computation of Hamiltonian matrix elements (by a numerical integration method based on a partitioning of space and application of product Gauss rules), (b) the approximation of integrals over the Brillouin zone (by the quadratic tetrahedron method), (c) the evaluation and processing of the Coulomb potential (via a density-fitting procedure), and (d) the expansion of one-particle states in suitable basis functions (numerical atomic orbitals, Slater-type exponential functions, and plane waves). Absolute precision and convergence are demonstrated for all these aspects and show that the method is a well-suited tool for unambiguous investigations of the density-functional approximation itself. Attention is given, in particular, to basis-set questions. Although the method is of the mixed-basis type, it is demonstrated that plane waves are not necessary; this holds for metals as well as for insulators and semiconductors. By a general prescription, sequences of accurate linear-combination-of-atomic-orbital (LCAO) basis sets can be defined that systematically approach the basis-set limit. This enables the routine application of the inherently efficient LCAO method to all kinds of systems. Exemplary calculations are performed on bulk Si-, *g*-C (graphite), Na, Ni, Cu, and NaCl, and on a hexagonal monolayer of weakly interacting O<sub>2</sub> molecules.

### I. INTRODUCTION

This paper describes a method for density-functional (DF) calculations on periodic systems, with periodicity in one, two, or three directions (*n*-dimensional crystals, *n*=1,2,3). To date several methods for DF calculations have appeared in the literature.<sup>1-13</sup> The chosen approaches often put restrictions, however, on the achievable precision. The major problems are related to (a) the evaluation of (Hamiltonian) matrix elements, (b) the treatment of the [Coulomb and exchange-correlation (XC)] potential, (c) the integrations over the first Brillouin zone (BZ) in reciprocal space, and (d) the basis functions in which the one-electron states are expanded. We have been able to remove all limitations to the extent that for all these fundamental aspects we have implemented efficient, accurate, and rapidly converging strategies. This makes our method a tool for unambiguous examinations of what the DF approximation may implicate for periodic structures, and, e.g., for a rigorous investigation of the merits and deficiencies of pseudopotentials. All types of symmetry and of periodicity (one, two, or three dimensions) can be handled.

(a) At the core of our approach lies a numerical integration scheme by which all integrals in real space are evaluated. When (exact) *analytical* integration methods are adhered to, the choice of basis functions and representation methods for the potential is severely restricted. This may give rise to slow convergence (and consequently to inherent inaccuracies) because the admissible functions have difficulty approximating efficiently the ideal behavior, e.g., near the nuclei. Employment of pseudopoten-

tials, making the valence wave functions smoother in the core region, alleviates this, but at the price of some arbitrariness and reduced interpretability of the results. If a *numerical* integration procedure is chosen throughout, relieving the restriction on basis functions and facilitating the evaluation of potential matrix elements, the accuracy can be a vexing problem. Virtually perfect schemes exist for the simplest systems, atoms and diatomic molecules, but not for three-dimensional systems. The Diophantine method,<sup>14,15</sup> for instance, easily applicable to all kinds of systems, hardly reaches two or three significant digits;<sup>16</sup> this may suffice in many cases but it turns into a definite bottleneck when higher precision is needed in the analysis of subtle effects and weak interactions. The numerical scheme we employ is based on a judicious partitioning of space and subsequent application of Gauss-type integration rules for the obtained subregions.<sup>17,18</sup> This results in high precisions and rapid convergence with the number of points, which puts all associated aspects of the calculation well under control.

(b) The long history of shape approximation methods (muffin tin, overlapping spheres) illustrates the difficulties involved in the treatment of the Coulomb potential. By now it is widely recognized that a close correspondence between the charge density and the Coulomb potential that is computationally derived from it is of crucial importance for reliable results; the past decade has witnessed various efforts to improve existing methods in this respect.<sup>8,19-21</sup> In our setup the Coulomb potential is evaluated via an expansion of the charge density in suitable function sets.<sup>22</sup> The variational freedom of these sets is easily increased and the rapid convergence in the

approximation eliminates effectively all problems and imperfections in the computation and processing of the Coulomb potential.

(c) All methods for numerical integrations over the BZ in  $k$  space give fair results for the easy integrals: the charge densities in insulators and semiconductors. More difficulties, both in absolute accuracy and in convergence, are encountered when the occupied bands are cut by Fermi surfaces. The calculation of properties that depend on details of the density of states and on the proper treatment of van Hove singularities is a serious problem unless the adopted method is implicitly based on a sensible representation of the functional form of the energy bands. We perform integrations in  $k$  space with the quadratic tetrahedron method,<sup>23,24</sup> which will be shown to be accurate and to converge quickly for all types of systems, metals as well as insulators and semiconductors.

(d) Numerical integration of the matrix elements gives a considerable and, in principle, unlimited freedom in the choice of the basis functions for the one-electron states. We apply numerical atomic orbitals, analytic ("Slater-type") exponential functions (without limitations on the angular quantum numbers), and plane waves. The combination of these types of functions leads to highly efficient basis sets which allow a rapid and convenient approach of the basis-set limit, as will be illustrated.

A brief discussion of these methodological aspects follows below. Next we illustrate the precision and convergence characteristics of the present approach. In particular the efficiency of linear combination of atomic orbitals (LCAO) versus plane-wave expansion bases will be investigated. Comparisons will be made to available fully numerical (i.e., basis-set-free) benchmark calculations, and to the state-of-the-art full-potential linearized-augmented-plane-wave (FLAPW) method. Finally we compute the usual quantities (cohesive energy, bulk modulus, equilibrium lattice constant) for a few well-known bulk systems: Si,  $q$ -C (graphite), Na, Ni, Cu, and NaCl.

## II. METHOD

In the Kohn-Sham approach of the DF theory<sup>25,26</sup> the equation for the electron states in a periodic system reads

$$H\psi_n(\mathbf{k}; \mathbf{r}) \equiv [T + V_C(\mathbf{r}) + V_{xc}(\mathbf{r})]\psi_n(\mathbf{k}; \mathbf{r}) = e_n(\mathbf{k})\psi_n(\mathbf{k}; \mathbf{r}) . \quad (2.1)$$

$T$  is the kinetic-energy operator,  $-\frac{1}{2}\Delta$  in (Hartree) atomic units,  $V_C$  is the total Coulomb potential, due to the nuclear charges and the electron cloud,  $V_{xc}$  is the XC potential, and  $\psi_n(\mathbf{k}; \mathbf{r})$  is the one-electron state with wave vector  $\mathbf{k}$  and band index  $n$ . We use for the XC potential the Vosko, Wilk, and Nusair (VWN) formulas,<sup>27</sup> based on electron-gas studies by Ceperley and Alder.<sup>28</sup> For the sake of comparison with other publications we apply sometimes the  $X\alpha$  form, the parametrized variation on Slaters original proposal for the XC potential.<sup>29</sup>

### A. Numerical integration

An important aspect of our method is the numerical integration scheme by which all integrals over the crystal unit cell are evaluated. The points and weights of the integration formula are generated according to a scheme which is extensively discussed elsewhere.<sup>17,18</sup> The global approach is as follows. Space is partitioned into atomic cells (polyhedra) and inside each polyhedron an atomic sphere is chosen. Integration over the atomic spheres is done by a product of Gauss formulas for the radial and angular variables, respectively. To handle the remaining parts inside the polyhedra, each polyhedron is subdivided into pyramids, which have their top at the atom and as bases the respective faces of the polyhedron; the pyramids are thus truncated at their top by the atomic sphere. By a suitable coordinate transformation a truncated pyramid is transformed into the unit cube so that product Gauss-Legendre rules can be applied.

The numbers of integration points are optimized in each individual sphere and in each (truncated) pyramid such that a series of typical "atomic" one-center test functions are integrated with some prescribed precision. This is formalized by an integration parameter  $A$ : the number of points is determined such that the integrals of all test functions are computed with a relative error  $\leq 10^{-4}$ . When the points and weights are applied in electronic-structure calculations, the resulting precisions turn out to be comparable for most polyatomic systems.  $A=3$  leads usually to moderate accuracy and increasing  $A$  to 3.5 or 4 yields fair precision (better than  $10^{-3}$  a.u., say, in cohesive energies); typical numbers of integration points (per atom) for these settings range from 2000 to 5000. In the section on computational results we give examples of absolute precision and convergence of molecular integrals in relation to  $A$ .

### B. Basis functions

The fully numerical Herman-Skillman (HS) program<sup>30</sup> is used to solve the DF equations for the spherically symmetric free atoms from which the crystal is built up. As basis functions are employed the numerical atomic orbitals (NAO's) from the HS program, Slater-type orbitals (STO's), and (in three-dimensional crystals) plane waves (PW's). Either of these, or a combination of them, can be used. To obtain a function basis at a particular point  $\mathbf{k}$  of the BZ,  $\mathbf{k}$ -adapted Bloch functions are constructed from the atomic one-center functions (NAO's and STO's),

$$\phi(\mathbf{k}; \mathbf{r}) = \sum_{\mathbf{R}} e^{i\mathbf{k} \cdot \mathbf{R}} \chi(\mathbf{r} - \mathbf{R} - \mathbf{s}_{\alpha}) . \quad (2.2)$$

$\chi$  is a NAO or STO centered on atom  $\alpha$  at position  $\mathbf{s}_{\alpha}$  in the crystal unit cell; the summation runs over all lattice points  $\mathbf{R}$ . The PW's pertaining to  $\mathbf{k}$  are the functions  $e^{i(\mathbf{k} + \mathbf{K}) \cdot \mathbf{r}}$ , where  $\mathbf{K}$  is a point of the reciprocal Bravais lattice. The frozen-core approximation is optionally used for the innermost atomic states.

The availability of NAO's and STO's opens the way to flexible and highly efficient basis sets. The NAO's provide a reasonable first approximation to the atomic states in reaction with other atoms and adding one STO per

NAO gives the variational freedom to accommodate the relaxation. The detailed radial behavior of the added STO turns out to be of limited importance: it is the variational freedom that counts in the first place.

Substantial improvement on double- $\zeta$  sets (to be understood here as a NAO plus one STO for every occupied free-atom state) is obtained by adding polarization functions: STO's with higher angular-momentum quantum numbers. Also here it is found that the detailed radial behavior is not crucial and the major improvement in basis-set quality comes from the increased variational freedom in the *angular* variable. Convergence is fast when we go to higher- $l$  values and summarizing we may state that double- $\zeta$  sets plus one or two polarization functions yield results not far from the basis-set limit (say deviations  $\lesssim 10^{-3}$  a.u., in cohesive energies per atom).

In relatively open structures, such as small molecules, basis-set requirements are somewhat more stringent and triple- $\zeta$  (plus polarization) sets may be needed to achieve really high precision, as we will see. That such is not the case in more dense systems like three-dimensional (3D) crystals is presumably due to the basis functions centered on surrounding atoms providing the additional flexibility which must otherwise come from the triple- $\zeta$  quality.

In bulk crystals the PW's provide an alternative for basis-set improvement. The obvious advantage of PW's over atomic one-center functions is that the convergence to the basis-set limit can be monitored in a rigorous way (in principle). Starting, e.g., with a small LCAO set PW's can be added systematically. From a comparison of the two alternative approaches we find that the pure LCAO double- $\zeta$  plus polarization set performs very well, showing that PW's, or composite bases, are not necessary to obtain high precision. This holds for metals as well as for other systems.

### C. $k$ -space integration

For the BZ integrations we employ the quadratic tetrahedron algorithm. In this approach<sup>23,24</sup> the BZ is partitioned in (small) tetrahedra (triangles in two dimensions). The integration points are the vertices *and* the midpoints of the edges of all the tetrahedra. From the data in these points the energy bands *and* the functions to be integrated are approximated by quadratic forms over each tetrahedron, and hence piecewise quadratic forms over the whole BZ. The integrals of these quadratic forms are solved (piecewise) exactly. The precision can be increased by taking ever smaller tetrahedra to fill up the BZ. In the actual implementation this is controlled by a  $k$ -space integration parameter  $K$ , which is the number of sample points on any ray from the central point  $\Gamma$  to a vertex of the BZ (including the end points). The partitioning in tetrahedra and the requirement that also the midpoints of the edges are used implicates that  $K$  must be odd.

The piecewise quadratic approximations give theoretically a rapid convergence with increasing partitioning.<sup>23,24</sup> This is confirmed by our findings.  $K=3$  gives usually reasonable results,  $K=5$  is accurate enough in most cases, and with  $K=7$  the results are completely con-

verged for virtually all practical purposes. For the sake of comparison we have also implemented the *linear* tetrahedron method:<sup>31,32</sup> partitioning in tetrahedra (respectively, triangles) but using as sample points only the vertices, not the midpoints of the edges. In that case there is no restriction on  $K$ : it may be odd or even.

### D. Coulomb potential

The HS program provides the Coulomb potentials  $V_\alpha$  due to the spherically symmetric atomic densities  $\rho_\alpha$  plus nuclear charges  $Z_\alpha$ . Defining the deformation density  $\rho_{\text{def}}$  as the difference between the crystal charge distribution and the superposition of atomic densities gives for the crystal Coulomb potential

$$V_C(\mathbf{r}) = \sum_\alpha V_\alpha(\mathbf{r}) + \int \rho_{\text{def}}(\mathbf{r}') |\mathbf{r} - \mathbf{r}'|^{-1} d\mathbf{r}' . \quad (2.3)$$

The form in which  $\rho_{\text{crystal}}$  and hence  $\rho_{\text{def}}$  is obtained, i.e., as a summation over products of basis functions, precludes an analytical evaluation of the second term, while the singularity of the denominator makes the application of a numerical integration scheme unsuitable. The problem is solved by a density-fitting procedure.<sup>22</sup> A set of fit functions  $f_i$  is chosen such that (a) the density  $\rho_{\text{def}}$  can accurately be expanded in them and (b) the corresponding Coulomb potentials  $f_i^c$  are easily evaluated:

$$\rho_{\text{def}}(\mathbf{r}) \approx \sum c_i f_i(\mathbf{r}) , \quad (2.4)$$

$$V_C(\mathbf{r}) \approx \sum_\alpha V_\alpha(\mathbf{r}) + \sum c_i f_i^c(\mathbf{r}) . \quad (2.5)$$

The fit coefficients  $c_i$  are determined by a least-squares solution of Eq. (2.4) with the constraint that the total amount of charge in the right-hand side (rhs) is zero. As fit functions we employ atomic "Slater-type" exponential functions  $r^{n-1} e^{-\alpha r} Y_{lm}(\Omega)$ , the Coulomb potentials of which are easily computed.<sup>18,22</sup>

Although the charge density in general cannot be fitted exactly in this way, the precision can be made very high, especially by using angular-quantum numbers up to  $l=3$ , 4, or 5 in the fit set. In practice one uses large  $l=0$  and 1 sets (such that the radial variational freedom is almost saturated), several  $l=2$  functions, and one or two  $l=3, 4$  functions on every atom. The unlimited flexibility of this type of function sets, in particular with regard to the angular behavior, implies that no fundamental restricting (shape) approximations are made to the potential.

### E. Madelung sums

The one-center fit functions and the corresponding potential functions are combined into  $\mathbf{k}=0$  Bloch sums (2.2) to describe the periodic charge density in the crystal and its Coulomb potential. Due to the exponential decay of the fit functions their Bloch sums can be computed for any evaluation point  $\mathbf{r}$  as a quickly converging summation over lattice points in direct space. This does not hold for the potential functions, however. The potential of a fit function, a charge distribution characterized by

the angular-quantum number  $l$ , decays asymptotically as  $1/r^{l+1}$ . Its Bloch sum gives rise to the familiar lattice summations. Many methods exist to deal with the divergence and conditional convergence problems related to it.<sup>18,33–38</sup> One of the simplest approaches, easily applicable to all types of multipole lattice sums, is to use screening. A well-known screening function is the exponential function  $e^{-\alpha r}$ : one replaces the Coulomb potential  $1/r$  by  $e^{-\alpha r}/r$  and considers the results in the limit  $\alpha \rightarrow 0+$ . We employ another screening function  $h(r)$  to evaluate the lattice sums by a (screened) summation over real-space lattice points. The functional form of  $h(r)$  is the Fermi-Dirac function

$$h(r) = \frac{1}{1 + e^{(r - r_0)/d}}. \quad (2.6)$$

All multipole lattice sums are then evaluated by weighting the contribution from a given distance  $r$  by  $h(r)$ . The function  $h(r)$  decays exponentially for large  $r$ , which makes the lattice sums nicely converging. However, by choosing the cutoff parameter  $r_0$  sufficiently large, compared with the smoothness parameter  $d$ , the first few terms in the lattice sum are only negligibly affected by the screening and this turns out to be an advantage in the convergence behavior: in a practical application one cannot reach the limit of vanishing screening and the results are therefore only approximations of the limiting values. Ideally one would set both  $d$  and  $r_0$  (and  $r_0/d$ ) as large as possible. The computational costs of the lattice sum evaluations restricts this of course and in practice  $d$  is taken in the order of a few atomic units and the cutoff parameter  $r_0$  something like 40 a.u. These parameters are automatically set larger (smaller) in our program, leading to better (worse) approximations depending on the numerical integration parameter  $A$  discussed before;  $A$  determines thus the precision of a calculation in a more general sense than just via the numerical integration scheme.

The errors introduced by the finiteness of the screening can be judged by a comparison of computed Madelung constants with the known exact values. We have done this for a few standard crystal structures. The results are displayed in Table I for the accuracy values  $A=2$  and 4 and show that the errors introduced by the approximations are very small and converge quickly with increasing  $A$ .

#### F. Energy

The total energy is given by a sum of the kinetic, XC, and Coulomb energies:  $E = E_T + E_{xc} + E_C$ . There are

two sources of error in the computation of the energy. The first is from the evaluation of various integrals. The applied numerical integration procedure, though fairly accurate, is not exact. The second source of error is the fit functions used for the evaluation of the Coulomb potential, implicit in the Coulomb energy  $E_C$ . In general, the fitting cannot be exact and the difference between the exact (deformation) density and the fit density implicates an error in the computed Coulomb energy term.

The cohesive energy is the difference between the total energies of the crystal and the constituting atoms, respectively,

$$E_{coh} = \sum_{\alpha} E_{\alpha} - E_{\text{crystal}}. \quad (2.7)$$

The HS program determines the first term in the rhs of (2.7) almost exactly. The second term, the crystal energy, might be calculated by numerical integration of the appropriate integrals in the crystal integration grid. Since  $E_{coh}$  may be very small compared with the two terms defining it, care is needed lest a meaningless value for  $E_{coh}$  is obtained, even when  $E_{\text{crystal}}$  is computed with a relative error of  $10^{-4}$  or  $10^{-5}$ . Therefore we will rewrite (2.7) in a form that allows the calculation of  $E_{coh}$  directly by numerical integration, with corresponding precision. The crystal total energy is then defined and computed as

$$E_{\text{crystal}} = \sum_{\alpha} E_{\alpha} - E_{coh}. \quad (2.8)$$

The HS program yields all atomic functions in the form of function tables  $f(r_i)$ , specifying the values in a (dense) grid of radial values  $r_i$ . By interpolation from these tables the free-atom functions are evaluated in the crystal integration points. The various energy terms in  $E_{\text{coh}}$  are conceptually the difference of the corresponding terms in the crystal and atomic total energies, respectively. Since these can now be computed by integration of the energy densities in the same grid, the obtained difference term is identical to the integral of the difference function. Hence the precision of the integration is preserved in  $E_{coh}$ .

It may be stressed here that by numerical integration of different terms of the interaction energy in the same integration grid any (analytic) cancellation of large and opposite terms is automatically taken care of, since we integrate effectively the combined term. This applies, for instance, to the kinetic and Coulomb parts of the relaxation energy (the energy corresponding to the change in the electronic density from the sum-of-free-atoms situation to the self-consistent crystal). The automatic treatment of large and opposite (kinetic and Coulomb) terms,

TABLE I. Computed Madelung constants for different accuracies  $A$  (see text).

	Rocksalt	Cesium chloride	Zinc blende	Fluorite
$A=2$	1.747 514 1 . . .	1.017 654 1 . . .	1.637 761 2 . . .	2.519 084 0 . . .
$A=4$	1.747 561 9 . . .	1.017 679 5 . . .	1.638 063 4 . . .	2.519 400 7 . . .
Exact	1.747 564 59 . . . <sup>a</sup>	1.017 680 75 . . . <sup>a</sup>	1.638 05 . . . <sup>b</sup>	2.519 39 . . . <sup>b</sup>

<sup>a</sup>Reference 38.

<sup>b</sup>Reference 39.

an important point requiring special attention and careful algebraic manipulation in other approaches,<sup>9,11</sup> is a marked advantage of numerical integration methods. The kinetic and XC energies are computed from the usual expressions, where the latter depends, of course, on the density functional adopted.

For the Coulomb term of the cohesive energy let  $\rho_\alpha$  and  $V_\alpha$  be the density Coulomb potential (including the nuclear potential) of atom  $\alpha$  located at  $\mathbf{R}_\alpha$ . The deformation density  $\rho_{\text{def}} = \rho_{\text{crystal}} - \rho_{\text{atoms}}$  is approximated with fit functions for the solution of Poisson's equation:  $\rho_{\text{def}} = \rho_{\text{fit}} + \delta$ . Then

$$2\Delta E_C \equiv \int \int d\mathbf{r}_1 d\mathbf{r}_2 \left[ \rho_{\text{crystal}}(\mathbf{r}_1) + \sum_\alpha Z_\alpha \delta(\mathbf{r}_1 - \mathbf{R}_\alpha) \right] \frac{1}{r_{12}} \left[ \rho_{\text{crystal}}(\mathbf{r}_2) + \sum_\alpha Z_\alpha \delta(\mathbf{r}_2 - \mathbf{R}_\alpha) \right] \\ - \sum_\alpha \int \int d\mathbf{r}_1 d\mathbf{r}_2 [\rho_\alpha(\mathbf{r}_1) + Z_\alpha \delta(\mathbf{r}_1 - \mathbf{R}_\alpha)] \frac{1}{r_{12}} [\rho_\alpha(\mathbf{r}_2) + Z_\alpha \delta(\mathbf{r}_2 - \mathbf{R}_\alpha)] \quad (2.9a)$$

(after some algebraic manipulation, and omitting the spatial arguments)

$$2\Delta E_C = \sum_{\alpha \neq \beta} \int V_\alpha(\rho_\beta + Z_\beta) d\mathbf{r} + 2 \int V_{\text{atoms}} \rho_{\text{def}} d\mathbf{r} + \int V_{\text{fit}}(\rho_{\text{def}} + \delta) d\mathbf{r} + \int \int d\mathbf{r}_1 d\mathbf{r}_2 \delta(\mathbf{r}_1) \frac{1}{r_{12}} \delta(\mathbf{r}_2). \quad (2.9b)$$

In the rhs of (2.9b) the first term is the electrostatic interaction between the unrelaxed free atoms. The second and third terms are the relaxation terms, respectively, the interaction of the deformation density with the sum-of-free-atoms potentials, and the (approximate) self-energy of the deformation density. The last term of (2.9b) cannot be computed; it is an error term resulting from the inadequacy of the fit functions to describe the (deformation) density exactly.

The electrostatic term is (usually) dominant in the cohesive energy and can easily be computed separately with high precision, as we will discuss presently. The two relaxation terms are evaluated by "normal" numerical integration. The splitting off and separate treatment of the electrostatic term has no negative bearing on the cancellation of numerical integration errors in the Coulomb and kinetic terms of the cohesive energy, since this cancellation pertains to the *relaxation* of the charge distribution from the sum-of-atoms situation to the self-consistent density of the crystal; the relaxation terms in the Coulomb energy are still evaluated by integration in the same grid as the kinetic relaxation term.

The electrostatic interaction between two spherically symmetric atoms  $A$  and  $B$  at positions  $\mathbf{R}_A$  and  $\mathbf{R}_B$  is

$$E_{\text{elstat}} = \int \int d\mathbf{r}_1 d\mathbf{r}_2 (\rho_A + Z_A) \frac{1}{r_{12}} (\rho_B + Z_B) \\ = \int V_A(\rho_B + Z_B) d\mathbf{r} \\ = Z_B V_A(\mathbf{R}_B) + \int V_A \rho_B d\mathbf{r}. \quad (2.10)$$

The last integral is easily evaluated numerically by using prolate spheroidal coordinates.<sup>40</sup> Let  $A$  and  $B$  be located along the  $z$  axis, at positions  $z = \pm a$ . Define coordinates  $u, v, \phi$  by

$$x = a \sinh(u) \sin(v) \cos(\phi), \\ y = a \sinh(u) \sin(v) \sin(\phi), \\ z = a \cosh(u) \cos(v). \quad (2.11)$$

Numerical integration can now be set up as a product formula in the variables  $(u, p, \phi)$  with  $p \equiv \cos(v)$ . The  $\phi$  integral yields a factor  $2\pi$  because the functions  $V_A(\mathbf{r})$  and  $\rho_B(\mathbf{r})$  are invariant for rotation around the  $z$  axis. So

$$\int V_A(\mathbf{r}) \rho_B(\mathbf{r}) d\mathbf{r} = 2\pi \int_0^\infty du \int_{-1}^1 dp J(u, p) \rho_B(u, p) \quad (2.12)$$

with Jacobian  $J(u, p) = a^3 \sinh(u) [\cosh^2(u) - p^2]$ . For neutral atoms the functions fall off rapidly as  $u$  goes to infinity, so that the upper limit on the  $u$  integration can be replaced by a suitable  $u_{\text{max}}$ . Numerical integration is then performed by a Gauss-Legendre product formula in  $u$  and  $p$  ( $n_u \times n_p$  points). For light atoms (up to the first series of transition metals say)  $n_u = 30$ ,  $n_p = 20$  give already accurate results. Heavier atoms require somewhat more points but still the electrostatic interaction energy can be calculated virtually exactly without much effort. The precision of the cohesive energy is determined by the other terms.

In case the crystal calculation is started up with ions, the electrostatic energy has to be split in two terms: the Madelung energy due to the effective ionic point charges plus the interaction between the neutral atoms. The latter has been treated above. The former is evaluated by a finite lattice sum in real space with the screening function  $h(r)$  discussed before (2.6).

An upper bound on the error term in (2.9b) can be determined for three-dimensional crystals. Let  $\delta$  have the Fourier expansion

$$\delta(\mathbf{r}) = \sum_{\mathbf{K}} \delta_{\mathbf{K}} e^{i\mathbf{K} \cdot \mathbf{r}}. \quad (2.13)$$

$\mathbf{K}$  runs over the reciprocal-lattice sites.  $\rho_{\text{def}}$  contains zero

charge, as does  $\rho_{\text{fit}}$  (and hence  $\delta$ ) because of the applied constraint in the fit (2.4). Hence  $\delta_0=0$  in (2.13). The Coulomb potential due to  $\delta(\mathbf{r})$  can be derived from (2.13) by Poisson's equation  $-\Delta V=4\pi\rho$ , yielding for the error term

$$\begin{aligned}\epsilon &= \int \int d\mathbf{r}_1 d\mathbf{r}_2 \frac{1}{r_{12}} \delta(\mathbf{r}_1) \delta(\mathbf{r}_2) \\ &= \int V_\delta(\mathbf{r}) \delta(\mathbf{r}) d\mathbf{r} \\ &= 4\pi \int \left[ \sum_{\mathbf{K}} \frac{\delta_{\mathbf{K}}}{K^2} e^{i\mathbf{K} \cdot \mathbf{r}} \sum_{\mathbf{K}'} \delta_{\mathbf{K}'} e^{i\mathbf{K}' \cdot \mathbf{r}} \right] d\mathbf{r} \\ &\leq \frac{4\pi}{K_{\min}^2} \int \delta^2(\mathbf{r}) d\mathbf{r}. \end{aligned}\quad (2.14)$$

$K_{\min}$  is the smallest nonzero vector of the reciprocal lattice. The integral  $\int \delta^2(\mathbf{r}) d\mathbf{r}$  is easily computed and has shown in practice that the fit functions routinely employed are adequate.

### G. SCF linearizations

In big calculations the computational costs of the SCF procedure are dominated by two parts. (a) The evaluation of the matrix elements of the potential, the iteratively changing part of the Hamiltonian, in every sample point of the BZ,

$$V_{pq}^k = \sum_{i=1}^N w_i V(\mathbf{r}_i) \phi_p^k(\mathbf{r}_i)^* \phi_q^k(\mathbf{r}_i). \quad (2.15)$$

$w_i$  is the weight of integration point  $\mathbf{r}_i$  and  $\phi_p^k$  is the  $p$ th basis function in the  $k$ th sample point of the BZ. With  $M$   $k$  points,  $n$  basis functions, and  $N$  integration points in real space, the computational effort is proportional to  $MNn^2$ . (b) The iterative construction of the density,

$$\rho(\mathbf{r}_i) = \sum_{k=1}^M \sum_{b=1}^B o_b(k) \left| \sum_{p=1}^n c_{bp}^k \phi_p^k(\mathbf{r}_i) \right|^2. \quad (2.16)$$

$o_b(k)$  are occupation numbers for the one-particle eigenstates;  $c_{bp}^k$  are the coefficients of the expansion in the basis functions. With  $B$  occupied bands the computational effort scales with  $MNnB$ , which is a little less than for the potential matrix elements, but of the same order.

A considerable saving of computer time is achieved when the involved multiple-loop structures in the computations can be circumvented. For both cases this is possible, be it only at some cycles of the iterative procedure. The integration points and the basis functions are fixed quantities and the only factors that change from cycle to cycle are the potential  $V(\mathbf{r})$  in (2.15), respectively, the occupation numbers  $o_b(k)$  and eigenstate coefficients  $c_{bp}^k$  in (2.16). The latter are combined in the density matrices  $P^k$  (one for each  $k$  point)

$$P_{pq}^k = \sum_{b=1}^B o_b(k) c_{bp}^k c_{bq}^k \quad (2.17)$$

from which follows the expression for the density [equivalent with (2.16)]

$$\rho(\mathbf{r}_i) = \sum_{k=1}^M \sum_{pq} P_{pq}^k \phi_p^k(\mathbf{r}_i)^* \phi_q^k(\mathbf{r}_i). \quad (2.18)$$

The potential matrix elements depend linearly on the potential function (2.15) and similarly the density depends linearly on the density matrices (2.18). So, if in the first case the current potential function  $V(\mathbf{r})$  is accurately described by a linear combination of potentials in previous cycles, then the same holds for the potential matrices  $V^k$  and, analogously, a linear combination of previous density matrices  $P^k$  defines the corresponding linear combination of density functions  $\rho(\mathbf{r})$ . Testing the accuracy of the approximations and constructing the linear combinations are computationally of minor importance because in all cases one or more of the cost-determining factors are absent.

The linear approximations have enhanced the efficiency of our program considerably, in particular for computations on slowly converging systems. The number of cycles in which the approximations are not accurate enough, so that the exact potential and/or density have to be computed, does not vary so much from one system to another and has thus far always been between 5 and 50, with values in the range 5–15 being encountered the most frequently.

## III. COMPUTATIONS

In this section we will first demonstrate the precision and convergence behavior of the integration techniques in real space and in  $k$  space and show that these aspects are completely under control: with normal settings the errors are already very small and they can be reduced to any desired level without requiring unreasonable computational efforts. Having settled that point we will address basis-set questions. By tests against fully numerical (basis-set-free) and state-of-the-art FLAPW calculations and by comparisons with mixed basis sets we will see that in our method accurate LCAO basis sets are conveniently defined, which can in a well-prescribed way be extended to approach rapidly and efficiently the basis-set limit. Finally we will apply our approach to compute a few bulk solids; in view of the accuracy analyses below the results can be taken as very close to the (local-) density-functional limit (errors in the cohesive energies  $\lesssim 0.002$  a.u., say).

### A. Integration in real space

We start with the integration method in real space and examine its performance in two types of systems. In the first place we take the bulk solids Na (bcc), Ni (fcc), Cu (fcc), NaCl, *g*-C (graphite), and Si. Figure 1 shows the errors in the cohesive energies as a function of the integration parameter  $A$  discussed before. As “exact” we have taken the supposedly converged  $A=8$  values. The convergence is found to be very good in general.

The bumpy and irregular character of the trends displayed in Fig. 1 is hard to explain in detail. Two causes probably play a major role here. (a) The test functions used to calibrate the integration scheme will in general not represent every aspect of the molecular in-

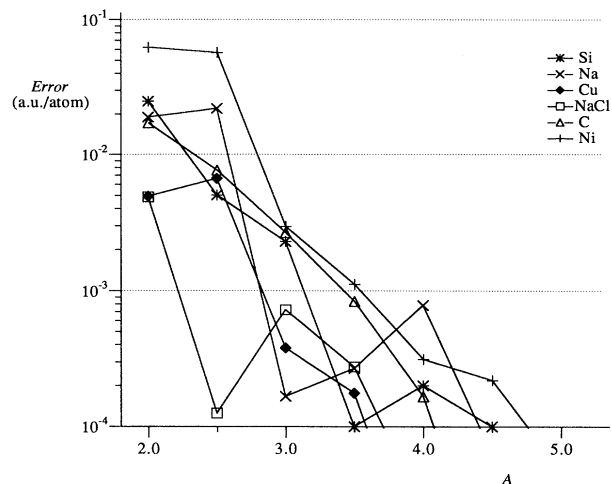


FIG. 1. Errors in cohesive energies (a.u./atom) as a function of the (real space) integration parameter  $A$  for the bulk solids Na, Ni, Si, Cu, NaCl, g-C, and Si.

tegrands to which the scheme is to be applied. Hence increasing the precision of the test integrals with a certain factor may occasionally change the final precision to a larger or smaller extent. (b) The testing algorithm monitors the relative integration precision in every individual atomic sphere and pyramid. The total precision then depends also on possible cancellations of the individual error terms. This cancellation effect is in its nature statistical and may therefore be expected to result in a somewhat bumpy behavior of the total error as a function of  $A$ . (c) The cohesive energy is a highly nonlinear function of various integrals, so that the error in it, and its convergence, cannot be expected to match in detail the integration errors. Also here, cancellation effects may play a role. Since the overall trend displays definitely a rapid convergence the irregularity is of minor importance.

In the second place we take periodic arrays of small diatomic molecules, CO or O<sub>2</sub>, with very large separations between neighboring molecules (30 a.u.). Three different periodic structures are employed for both CO and O<sub>2</sub>: (a) a three-dimensional simple cubic lattice with the molecules oriented along a coordinate axis, (b) a two-dimensional hexagonal array with the molecular axis orthogonal to the plane, and (c) a one-dimensional repetition where the molecules are aligned with the axis of periodicity. The geometry of these structures with their large empty spaces is far from ideal for the integration algorithms because several of the atomic pyramids that are generated in the scheme are very large (those directed towards neighboring cells) or very wide and flat (directed towards the partner atom in the cell). In such cases the integration method is put to a severe test: in the large pyramids because the relatively localized integrands are implicitly approximated by a slowly converging expansion in polynomials over the large region: in the very wide ones because the Jacobian of the transformation from a truncated pyramid to the unit cube approaches singularity.<sup>17,18</sup> The considered cases, though extreme, are not

academic: in chemisorption studies for instance, periodic overlayers of adsorbate molecules with large spacings may occur [cf. case (b)]. Figure 2 displays for all employed periodic structures the maximum errors in the one-particle energies as a function of  $A$  [the errors in the cohesive energies (not included) are in line with the presented data for the one-particle energies]. In spite of the geometric awkwardnesses the precision and convergence are reasonable, though markedly less indeed than for the more "homogeneous" bulk systems above. We conclude that accurate results are obtained in normal systems by setting  $A=3.5$  or 4.0. We will adopt therefore  $A=4$  as standard value; in geometrically suspect systems the integration precision should be checked and possibly increased.

## B. Integration in $k$ space

Next we consider accuracy and convergence of the integration in  $k$  space. We test this both for 3D BZ's (the bulk solids Na, Ni, Si, g-C, and NaCl) and for a 2D case [a single-layer Cu(100) slab]. Figure 3 gives the cohesive energy errors as a function of the integration parameter  $K$  introduced in the preceding section; the errors are defined as the deviations from the presumably  $K$ -converged values ( $K=9$ ). For a comparison we have used both our quadratic tetrahedron method (data for  $K$  odd) and the classical linear tetrahedron method ( $K$  even). The outcomes confirm the theoretical superiority of the quadratic approach<sup>23,24</sup> and henceforth we consider only the quadratic method. In all cases the convergence rates are very similar and the absolute precision is moderate for  $K=3$  ( $\sim 0.01$  a.u.), good for  $K=5$  ( $\sim 0.001$  a.u.), while the results for  $K=7$  can be considered converged for all practical purposes.

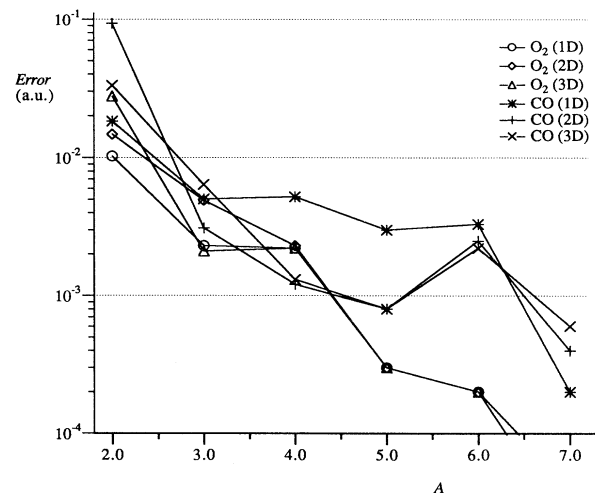


FIG. 2. Maximum errors in the one-electron energies (a.u.) in CO and O<sub>2</sub> "crystals", as a function of the integration parameter  $A$ . 1D, 2D, and 3D refer to one, two, and three-dimensional periodic structures (see text).

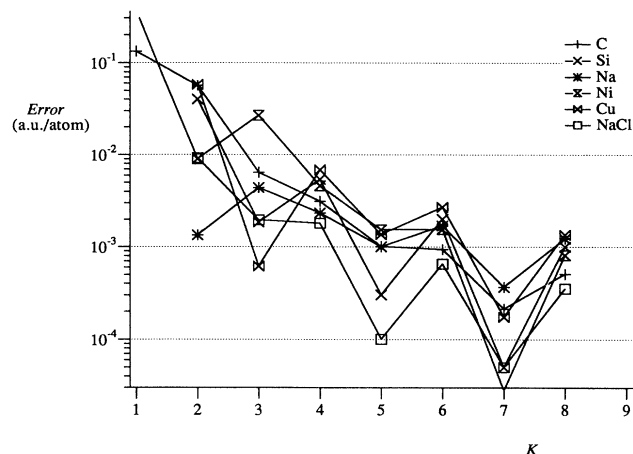


FIG. 3. Errors in cohesive energies (a.u./atom) as a function of the  $k$ -space integration parameter  $K$  for bulk Na, Ni, g-C, Si, and NaCl and for a one-layer Cu(100) slab.

### C. Basis set

To investigate basis sets we consider first the diatomic molecules CO and O<sub>2</sub>; they are computed effectively as isolated molecules because the separation with neighboring molecules is so large (30 a.u.) that intermolecular interactions are negligible. These systems are interesting as testing material because the local-density (LD) basis-set limit is presumably known, cf. the fully numerical results

for diatomic molecules.<sup>41-43</sup> Near-dependency of basis sets, often feared as a worrying feature in LCAO solid-state methods, is of minor importance in isolated molecules, so that we can extensively investigate basis-set effects. For CO an elaborate analysis of basis sets in LCAO calculations is known,<sup>44</sup> in which the Amsterdam DF molecular program was used, which is very similar to our band-structure program; this gives an additional check on our CO results and the basis-set analysis we will perform for O<sub>2</sub> can be compared with the results found previously for CO.

We start with an all-electron high-quality basis set, which can be characterized as quadruple- $\zeta$  (double- $\zeta$  for the deep-lying 1s states) plus  $d$ - and  $f$ -polarization functions; the exponential decay factors have been taken even-tempered (approximately); for the polarization functions it was assumed that they should attain their maximum in the bond region, halfway the next atom or a little more contracted. The STO basis has been derived from Baerends *et al.*<sup>44</sup> For the oxygen atom we have replaced one STO by the corresponding NAO in the subsets for the occupied atomic states (1s, 2s, 2p). This does not affect the results with the high-quality basis. When considering smaller basis sets, however, as we will do next, it may be expected that the NAO's are able to describe to a large extent the behavior of the molecular orbitals in the core region so that the flexibility of the additional (Slater-type) functions can be utilized for the bond region. The specifications of the large basis are given in Table II, where also the characteristics of the fit functions (for the computation of the Coulomb potential) can be found.

TABLE II. Basis functions and fit functions for carbon and oxygen in CO and O<sub>2</sub>. NAO's are numerical orbitals from the free-atom program. All other entries refer to Slater-type exponential functions  $r^{n-1}e^{-\alpha r}Y_{lm}(\Omega)$ ; the leftmost column specifies the quantum numbers ( $n,l$ ); the exponential decay factors  $\alpha$  are given in the other columns.

TABLE III. One-particle energies (a.u.) for the diatomic molecules CO and O<sub>2</sub>. Present calculations: periodic structures with intermolecular separation 30 a.u.

Orbital	CO			Orbital	O <sub>2</sub>		
	Numerical calculations <sup>a</sup>	Present	Molecular calculations <sup>b</sup>		Numerical calculations <sup>a</sup>	Present	
1σ	-18.7442	-18.7446	-18.7448	1σ <sub>g</sub>	-18.7856	-18.7832	
2σ	-9.9114	-9.9115	-9.9122	1σ <sub>u</sub>	-18.7855	-18.7831	
3σ	-1.0442	-1.0451	-1.0461	2σ <sub>g</sub>	-1.1665	-1.1652	
4σ	-0.4891	-0.4890	-0.4903	2σ <sub>u</sub>	-0.6870	-0.6850	
5σ	-0.3030	-0.3040	-0.3036	3σ <sub>g</sub>	-0.4607	-0.4585	
1π	-0.4126	-0.4127	-0.4137	1π <sub>u</sub>	-0.4481	-0.4462	
2π*		-0.0505	-0.0506	1π <sub>g</sub>	-0.1882	-0.1862	

<sup>a</sup>Reference 43.

<sup>b</sup>Reference 44.

For a comparison with the fully numerical results of Laaksonen, Sundholm, and Pyykkö<sup>43</sup> the  $X\alpha$  formula, with parameter value 0.7, is used for the XC functional and spin polarization is not allowed, i.e., the calculations are performed “spin restricted.” The atomic separations are 2.27 a.u. for O<sub>2</sub> and 2.13 a.u. for CO. In Table III we give the one-electron energies from which it is clear that our basis sets for carbon and oxygen are fairly complete. The deviations in the one-electron energies from the numerical values are roughly 0.002 a.u. and even less for CO. The agreement with the values of Baerends *et al.*<sup>44</sup> for CO is as it should be, since essentially the same method and basis have been used; it serves as a check and shows besides that the employment of oxygen NAO’s, instead of one more STO for 1s, 2s, and 2p, does not make much difference in this basis.

We have also calculated O<sub>2</sub> with the slightly larger O–O distance 2.282 a.u. for a comparison with precise FLAPW computations,<sup>8</sup> which can be considered state-of-the-art for plane-wave-type approaches. In Ref. 8 a 2D hexagonal array of upright molecules was used, separated by 6.846 a.u.; we have employed the same geometry as well as the 2D hexagonal array with the larger intermolecular separation of 30 a.u. as in our other computations. Assuming that the same high level of precision applies to these O<sub>2</sub> calculations with the larger O–O distance 2.282 a.u. as for the distance 2.27 a.u. above,

the quality of the FLAPW data can be assessed. The results are presented in Table IV and Fig. 4. For the smaller intermolecular separation there is a non-negligible interaction between neighboring molecules, giving rise to dispersion, i.e., to bands, so that a single value of molecular one-particle energies does not apply. The energy values of Ref. 8 are the eigenvalues at the  $\Gamma$  point.<sup>45</sup> Taken as data for an isolated molecule (as they were presented in Ref. 8) all FLAPW σ energies are close to the limiting values, with errors of a few milli-atomic-units but the two π states are too high by ~0.014 a.u. However, in fairness the comparison should be made to a periodic structure calculation, in which the intermolecular interaction is taken into account. The  $\Gamma$  eigenvalues are then the lowest values in the σ bands and the highest in the π bands. Now it turns out (Fig. 4, Table IV) that the complete FLAPW spectrum is shifted upward by no less than ~0.015–0.020 a.u. (~0.5 eV). We do not know the reason for this shift; probably the field caused by the incomplete screening of the surrounding oxygen nuclei is not fully taken into account. Another possibility (not completely ruled out by the information in Refs. 8 and 45) is that only the  $\Gamma$  point is used in the computation, so that the integrations over the BZ have in fact been simplified too much. In Fig. 4 (leftmost part) we have also plotted the outcome of such a simplification: a no-dispersion, molecularlike spectrum, shifted upward (by

TABLE IV. One-particle energies for 2D O<sub>2</sub> crystals with intermolecular separations of 30 and 6.846 a.u. for comparison with FLAPW results.

Orbital	Present		FLAPW <sup>a</sup> <i>D</i> =6.846 a.u.	Present <i>D</i> =30 a.u. (isolated)
	<i>D</i> =6.846 a.u. Γ-point values			
1σ <sub>g</sub>	-18.8044		-18.789	-18.7839
1σ <sub>u</sub>	-18.8043		-18.789	-18.7838
2σ <sub>g</sub>	-1.1775		-1.1545	-1.1602
2σ <sub>u</sub>	-0.7040		-0.6905	-0.6871
3σ <sub>g</sub>	-0.4764		-0.4615	-0.4582
1π <sub>u</sub>	-0.4509		-0.4295	-0.4442
1π <sub>g</sub>	-0.1957		-0.175	-0.1883

<sup>a</sup>Reference 8.

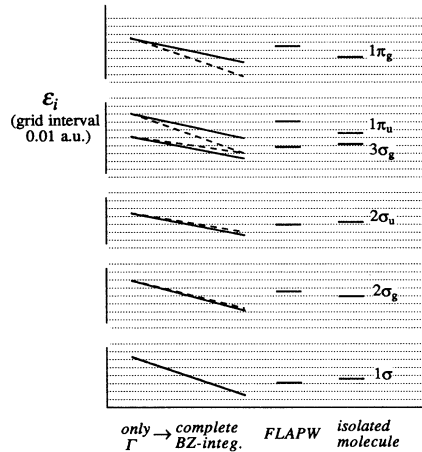


FIG. 4. Comparison of one-particle energies in  $O_2$ . The one-particle states have been shifted relative to each other to enable an overview in one picture. The gaps in the energy axis separate the distinct parts of the spectrum. Right (isolated molecule): present periodic structure calculation with large intermolecular separation (30 a.u.). Middle (FLAPW): calculation of Ref. 8 for periodic structure with intermolecular separations 6.846 a.u.; eigenvalues at  $\Gamma$ . Left: present periodic structure calculation with molecular separation 6.846 a.u. Leftmost: computation with only the  $\Gamma$  point for BZ integrations, giving a discrete spectrum. Rightmost: correct BZ integrations used: single states broaden into bands; the  $\Gamma$ -point eigenvalues are the lowest in the  $\sigma$  bands and the highest in the  $\pi$  bands; these are indicated as solid lines.

$\sim 0.020$  a.u.) with respect to the isolated molecule. The reason for this computational effect is easily understood: the major dispersion effects are displayed by the  $\pi$  bands, so that the error caused by simplifying BZ integrals (to compute the charge density) to the  $\Gamma$  point only, is dominated by representing the  $\pi$  bands only by the antibonding  $\mathbf{k}=0$  combination. This contracts the ( $\pi$ -) charge density too much onto the nuclei, the nuclear potentials are spuriously screened, and the one-electron eigenenergies are raised.

We proceed to assess what aspects of the basis are primarily responsible for the high quality. We do so for  $O_2$  (with the O-O distance 2.27 a.u. and with large separations between the molecules). Table V defines a sequence of basis sets for  $O_2$ . Set 1 is the “limit” set defined in Table II and used for Tables III and IV. In set 2 the two  $3d$  polarization functions are replaced by one (with intermediate exponential factor). In set 3 we reduce in addition the  $s$  and  $p$  sets from quadruple- $\zeta$  to triple- $\zeta$  quality; this basis will turn out to be an interesting one: the smallest accurate basis. We assess the minimality of that basis by reducing the  $s$  and  $p$  sets to double- $\zeta$  quality (bases 4 and 5), or by removing the  $4f$  and  $3d$  polarization functions (6 and 7). In all cases the basis-set errors increase significantly. Sets 8 through 11 are variations on (the minimal accurate) set 3 in the sense that the exponential decay factors of the STO’s are varied. In basis 12 finally the frozen-core approximation is used for the oxygen  $1s$  state; this hardly changes the outcomes at all.

Figure 5 displays the maximum errors in the one-particle energies and the cohesive energies, defining the results with set 1 as exact. It has been established<sup>44</sup> that for CO a triple- $\zeta$   $s,p$  set plus one  $3d$  and one  $4f$  function (for each atom) represents almost the basis-set limit and reduction of one of the components seriously affects the results. We find the same for  $O_2$ . The exponential decay factors turn out to be noncritical: variations within reasonable limits keep the results within the overall basis-set accuracy range. This is an interesting and welcome notion because it means that for accurate calculations time-consuming basis set optimizations are not necessary. It opens the way to a routine choice of high-quality LCAO basis sets. Naturally in less precise computations with smaller basis sets the detailed choice of functions may be more critical, but this means only that the results of such calculations are inherently unreliable. We conclude that a (minimal) accurate basis consists of triple- $\zeta$   $s$  and  $p$  sets and two polarization functions. The decay factors of the latter are to be chosen such that their maxima are  $\sim 0.4$  times the bond length; the triple- $\zeta$  sets contain one contracted and one diffuse function in addition to the NAO.

TABLE V. Different basis sets for  $O_2$  used to analyze the essence of “high quality” in LCAO bases. Entries between parentheses refer to other sets; set (1) has been defined in Table II.

Basis	1s	2s	2p	3d	4f		
(1)	NAO 6.80	NAO 5.87 1.70	4.31	NAO 7.56 1.14	3.45	2.96 1.69	2.50
(2)	(1)		(1)		(1)	2.00	(1)
(3)	(1)	NAO 4.31	1.70	NAO 4.08	1.12	(2)	(1)
(4)	(1)	NAO 1.70		NAO (3)		(2)	(1)
(5)	(1)	NAO 1.70		NAO 1.30		(2)	(1)
(6)	(1)	(3)		NAO (3)		(2)	
(7)	(1)	(3)		NAO (3)			
(8)	(1)	(3)		NAO (3)		1.80	2.25
(9)	(1)	(3)		NAO (3)		2.50	3.75
(10)	(1)	(3)		NAO (3)		2.20	3.20
(11)	(1)	NAO 4.00	1.40	NAO 4.00	1.20	2.20	3.20
(12)	frozen	(11)		(11)		(11)	(11)

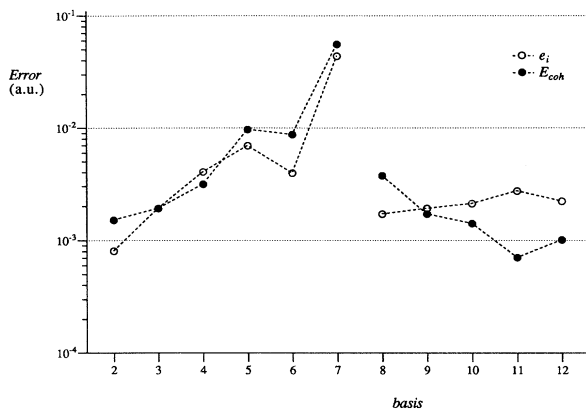


FIG. 5. Errors in the cohesive energy and the one-electron energies (a.u.) in  $O_2$  for several basis sets, defined in Table V.

We turn now to bulk solids and examine basis sets in Si,  $g$ -C, Na, Ni, Cu, and NaCl. These represent a fair variety: covalent bonding, simple and transition metals, and ionicity. We cannot completely repeat the analysis used for  $O_2$  because large “molecular” valence sets (triple  $\zeta$  or even quadruple  $\zeta$ ), incorporating diffuse functions, cause dependency problems in the Bloch basis due to the accumulated overlaps with functions on surrounding atoms. Furthermore, the basis-set limit is not known and from a principal point of view LCAO methods seem unsuitable for a well-defined *systematic* approach of this limit.

The first point makes it probable that double- $\zeta$  sets might be sufficient, as the reduced one-center variational freedom may be compensated by the presence of functions on nearby atoms. The second problem can be attacked by the application of plane waves. The following approach is therefore chosen. We define as the starting point a double- $\zeta$  (naturally: one NAO plus one STO) valence set without polarization functions, which will be denoted the *basic* set; the frozen-core approximation is used for the innermost atomic states. Then we add polarization functions and monitor convergence (the cohesive energy is used to compare results). The polarization

functions that give too small improvements, less than 0.001 a.u./atom say, are removed again and we have obtained a presumably accurate LCAO set, which will be called the *full* (LCAO) basis. For a comparison we add also *plane waves* to the basic set and monitor convergence of *that* sequence. Finally we add plane waves to the *full* set and check in this way whether we have been missing important components in the LCAO basis (which proves not to be the case).

The plane-wave sequences are defined by adding the waves in “stars” of reciprocal-lattice points. The polarization STO’s to be supplemented have exponential decay factors  $\alpha$  such that the maxima of these functions are roughly at 0.33–0.40 times the nearest-neighbor distance. This is a little shorter than was found optimal for the  $O_2$  molecule. We have done so because in denser systems, like the bulk solids under consideration, only local features of the wave functions need to be described; further away the basis functions on other atoms take over. We have carried out a few pilot calculations and found the more contracted functions performing better, although the differences were small ( $\sim 0.002$  a.u. at most) for a fair range in exponent values; this points out once again that detailed radial characteristics are relatively unimportant for the basis-set quality.

Table VI contains the (STO parts of the) basic sets and the polarization functions. The latter are labeled by a star; those with a double star turn out to be unimportant and do not belong to the “full” LCAO basis. Figure 6 displays for the basis-set sequences defined above the cohesive energies as a function of the number of functions (per unit cell) added to the basis set; for each system a constant term has been added in order to enable a fine-scale overview of all cases in one picture: we consider here convergence and relative values rather than absolute ones. Adding plane waves to the *full* LCAO sets yielded changes in the cohesive energies smaller than 0.0015 a.u.; we do not show these data here.

The basis sets for Na have been used for the sodium crystal as well as for NaCl. As is apparent from Fig. 6 the Na polarization functions play no role in the sodium crystal. They are important, however, in NaCl; the single and double stars on the Na functions in Table VI refer to the latter. The polarization sequence for NaCl is defined

TABLE VI. STO characteristics for the *basic* sets and for the polarization functions (\*). Unimportant polarization functions are indicated by two stars (\*\*); see text.

Orbital	C	Si	Na	Ni	Cu	Cl
1s	(frozen)	(frozen)	(frozen)	(frozen)	(frozen)	(frozen)
2s	2.00	(frozen)	2.20	(frozen)	(frozen)	(frozen)
2p	2.00	(frozen)	2.20	(frozen)	(frozen)	(frozen)
3s		2.00	1.10	4.05	4.15	1.75
3p		1.60	1.10*	3.50	3.55	1.30
3d	1.90*	1.35*	1.10*	1.95	1.30	1.10*
4s				2.00	2.50	
4p				2.00*	1.85*	
4d						
4f	2.90*	2.00*	1.70**	2.00*	1.85*	1.70**
5g	3.80**	2.70**		2.60**	2.50**	2.20**

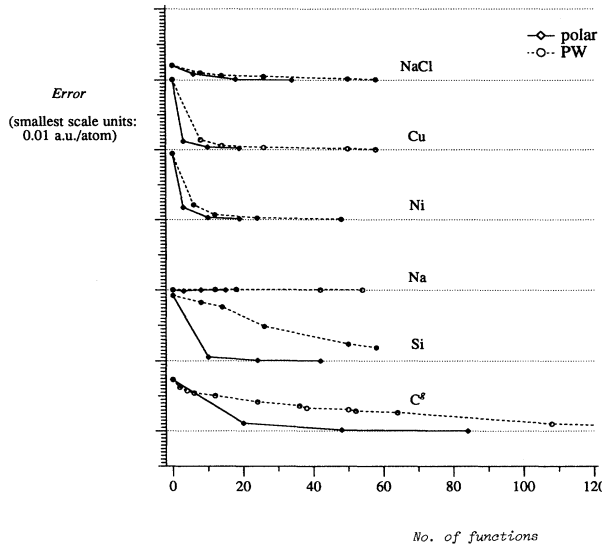


FIG. 6 Convergence of the cohesive energy errors (a.u./atom) for basis-set sequences. Abscissa: number of functions on top of the “basic” LCAO set. Polar: LCAO polarization functions added. PW: plane waves added (in stars of reciprocal-lattice points). The exact values are here defined as the best values obtained with the employed basis sets.

by taking at every step an additional function for each of the two atoms. With two polarization functions per atom the sequence is converged, but a test calculation showed that the 4f function on Cl was in fact irrelevant; hence the double star on it in Table VI.

Basis-set-free results are not available in these cases, as they were for the diatomics CO and O<sub>2</sub>. Furthermore, although the PW sequences are known formally to converge, it is not certain to what extent the limited sequences displayed in Fig. 6 have actually approached the limit. Nevertheless the data strongly suggest that the limit is approximated closely and we infer that (a) the polarization approach gives a very good convergence, two functions being usually necessary and sufficient to yield a highly precise result (the remaining basis-set error is  $\sim 0.001$  a.u. or better) and hence (b) the full LCAO basis is very adequate; in particular the polarization functions are important; they represent what alternatively the plane waves have to offer to a bare double- $\zeta$  basis. In the cases of g-C and Si the approach with polarization functions is significantly more effective than with the plane waves, but also for the metals and NaCl the PW approach does not match the LCAO method in efficiency. Mixed basis sets (PW's plus Gaussians) have been tested before for semiconductors<sup>46</sup> and for metals,<sup>47</sup> and it was found that one polarization function gives already very good results and that addition of a few plane waves on top of that basis produces virtually the limiting results (by comparison with large plane-wave sets); these findings fit in with our results.

As a last note we mention that in the computations on NaCl we start routinely up with neutral atoms. We have done a few comparative calculations by starting up with

ions ( $\pm 0.8e$ ). This implicates of course a different set of NAO's. Confirming the general trend of our findings, i.e., that the *flexibility* of the basis determines the quality, rather than details of individual functions, we found changes in the total crystal energy of only  $6 \times 10^{-4}$  a.u. (basic set +1PW) and  $5 \times 10^{-5}$  a.u. (basic set +2PW), i.e., the differences are small compared with the total basis-set error and disappear rapidly as the quality of the basis is improved.

#### D. Si, g-C, Na, Cu, Ni, NaCl

Finally we compute for the employed bulk crystals the usual physical quantities: the equilibrium lattice constant, bulk modulus, and cohesive energy. The full bases, as defined above, are used and the integration parameters have been set at high values  $A=5$ ,  $K=7$  ( $A=4$ ,  $K=5$  during geometry optimization) to remove any relevant integration errors. From the analyses above it will be clear that the results must be virtually converged with these settings. We have verified this by comparing with the results for “normal” integration settings  $A=4$ ,  $K=5$  in the equilibrium geometry. The cohesive energies change at most by 0.002 a.u., in qualitative agreement with Figs. 1 and 3.

The VWN formulas have been applied for the exchange-correlation functional. The lattice constant and the bulk modulus for the energy minimum are obtained by fitting the Murnaghan equation of state<sup>13,48</sup> to the energy values  $E(V)$  for different volumes  $V$ . From a moderate variation in volumes and hence in energy values, say a 20% range in lattice constants, the equilibrium volume is easily determined, using Murnaghan's equation or any other reasonable curve. For the bulk modulus, however, significantly different values are found if a simple polynomial fit of degree 2 (or 3 or 4) is used around the minimum. The problem of an *accurate* determination of  $B_0$  from a simple polynomial approximation has been noticed before.<sup>11</sup> Van Camp, Van Doren, and Devreeze<sup>49</sup> applied another “equation of state,” the equation of Birch,<sup>50</sup> and found differences with the Murnaghan results up to 4%; moreover, the Birch equation gave *smaller* moduli and a *better* fit in the cases they considered (diamond and silicon). We have used the Murnaghan equation to conform to the majority of workers in this field. When comparing to *experimental* values, however, one should keep this uncertainty in mind and allow for “error bars” in the order of a few percent. Murnaghan's equation is

$$E(V) = E(V_0) + \frac{VB_0}{B'(B'-1)} \left[ B' \left( 1 - \frac{V_0}{V} \right) + \left( \frac{V_0}{V} \right)^{B'} - 1 \right]. \quad (3.1)$$

$V_0$  is the equilibrium volume,  $B_0$  the bulk modulus, and  $B'$  its volume derivative.

The computed cohesive energies in Table VII have been corrected for the zero-point motion in the solids, which is contained in the experimental values, and they

TABLE VII. Cohesive energy ( $E_{coh}$ , a.u./atom), equilibrium lattice constant  $a_0$  (a.u.), bulk modulus  $B_0$  (Mbar), and (for Ni) the magnetic moment  $\mu$  ( $\mu_B$ /atom). The cohesive energy of NaCl is defined with respect to the ions ( $\pm 1e$ ). PP is pseudopotential and Sr is semirelativistic. Exchange-correlation functional employed in this work: VWN.

	Na			Cu			Ni			
	$E_{coh}$	$a_0$	$B_0$	$E_{coh}$	$a_0$	$B_0$	$E_{coh}$	$a_0$	$B_0$	$\mu$
Expt.	0.041 <sup>a</sup>	7.98 <sup>a</sup>	0.068 <sup>b</sup>	0.128 <sup>c</sup>	6.82 <sup>d</sup>	1.37 <sup>b</sup> 1.42 <sup>c</sup>	0.163 <sup>a</sup>	6.7 <sup>e</sup>	1.86 <sup>f</sup>	0.55 <sup>f</sup>
This work	0.044	7.71	0.086	0.157	6.71	1.67	0.215	6.52	2.44	0.552
Other DF calculations	0.041 <sup>a</sup> 0.045 <sup>h</sup>	7.69 <sup>a</sup>	0.09 <sup>a</sup>	0.150 <sup>a</sup> 0.149 <sup>e</sup> 0.123 <sup>i</sup> 0.173 <sup>h</sup> 0.141 <sup>k</sup> 0.152 <sup>l</sup> 0.144 <sup>m</sup>	6.77 <sup>a</sup> 6.8 <sup>e</sup> 6.85 <sup>c</sup> 6.71 <sup>j</sup> 6.84 <sup>k</sup> 6.82 <sup>l</sup> 1.29 <sup>e</sup> 1.86 <sup>j</sup> 1.80 <sup>h</sup> 1.88 <sup>k</sup> 1.62 <sup>l</sup>	1.55 <sup>a</sup> 1.29 <sup>e</sup> 1.50 <sup>c</sup>	0.210 <sup>a</sup>	6.55 <sup>a</sup> 6.6 <sup>e</sup>	2.27 <sup>a</sup> 2.09 <sup>g</sup>	0.68 <sup>g</sup>
HF	0.117 <sup>y</sup> 0.104 <sup>aa</sup>									

	Si			g-C			NaCl				
	$E_{coh}$	$a_0$	$B_0$	$E_{coh}$	$a$	$c$	$B_0$	$B_{isotr.}$	$E_{coh}$	$a_0$	$B_0$
Expt.	0.170 <sup>n</sup>	10.24 <sup>d</sup> 10.26 <sup>n</sup>	0.99 <sup>b</sup> 0.98 <sup>o</sup>	0.272 <sup>p</sup>	4.649 <sup>q</sup> 4.653 <sup>r</sup> 4.647 <sup>t</sup>	12.578 <sup>r</sup> 12.612 <sup>t</sup>	0.41 <sup>s</sup>	3.18 <sup>s</sup>	0.147 <sup>d</sup> 0.148 <sup>b</sup>	10.6 <sup>d</sup> 10.66 <sup>b</sup> 10.7 <sup>e</sup>	0.26 <sup>e</sup> 0.266 <sup>u</sup>
This work	0.193	10.259	0.95	0.320	4.62	12.26	0.38	3.09	0.162	10.36	0.315
Other DF calculations	0.172 <sup>v</sup> 0.180 <sup>x</sup> 0.209 <sup>y</sup> 0.183 <sup>z</sup> 0.178 <sup>n</sup> 0.200 <sup>aa</sup>	10.301 <sup>v</sup> 10.11 <sup>x</sup> 10.223 <sup>z</sup> 10.267 <sup>n</sup> 10.14 <sup>i</sup> 10.256 <sup>o</sup>	0.98 <sup>v</sup> 1.15 <sup>x</sup> 1.0 <sup>z</sup> 0.92 <sup>n</sup> 0.89 <sup>i</sup> 0.855 <sup>o</sup> 0.880 <sup>o</sup>	0.320	4.65 <sup>w</sup>	12.9 <sup>w</sup>	0.50 <sup>w</sup>	3.19 <sup>w</sup>	0.142 <sup>b</sup> 0.149 <sup>e</sup> 0.152 <sup>u</sup>	10.2 <sup>e</sup> 10.66 <sup>u</sup> 0.304 <sup>u</sup>	0.32 <sup>e</sup>
HF	0.117 <sup>y</sup> 0.104 <sup>aa</sup>										

<sup>a</sup>Reference 53: KKR, modified Hedin-Lundqvist.

<sup>b</sup>Reference 55.

<sup>c</sup>Reference 62: sr, pp, PW + GTO, Ceperley-Alder.

<sup>d</sup>Reference 54.

<sup>e</sup>Reference 7: ASW, modified Hedin-Lundqvist.

<sup>f</sup>Reference 74.

<sup>g</sup>Reference 73: KKR, von Barth-Hedin.

<sup>h</sup>Reference 64: spherical cellular, modified Hedin-Lundqvist.

<sup>i</sup>Reference 61: pp, PW, Ceperley-Alder.

<sup>j</sup>Reference 63: sr, ASW, modified Hedin-Lundqvist.

<sup>k</sup>Reference 65: pp, GTO, Hedin-Lundqvist.

<sup>l</sup>Reference 66: LAPW, Wigner formula.

<sup>m</sup>Reference 67: pp, PW.

<sup>n</sup>Reference 60: pp, PW, Wigner formula.

<sup>o</sup>Reference 49: pp, PW (two different equations of state), Wigner formula.

<sup>p</sup>Reference 69.

<sup>q</sup>Reference 68.

<sup>r</sup>Reference 71.

<sup>s</sup>Reference 72.

<sup>t</sup>Reference 75.

<sup>u</sup>Reference 59: FLAPW, Hedin-Lundqvist.

<sup>v</sup>Reference 56: pp, PW, Wigner formula.

<sup>w</sup>Reference 70: FLAPW, Hedin-Lundqvist;  $E_{coh}$  from computed total energy and our own atomic energy values.

<sup>x</sup>Reference 13: pp, GTO, Hedin-Lundqvist.

<sup>y</sup>Reference 57: LMTO, von Barth-Hedin.

<sup>z</sup>Reference 58: LMTO, modified von Barth-Hedin.

<sup>aa</sup>Reference 52: LMTO, HF/von Barth-Hedin.

are defined relative to spherically symmetric spin-polarized atoms in their lowest DF (VWN) state, e.g., for Ni:  $d^9s^1$ . (So multiplet splitting is neglected, the atomic energy is calculated too high, and hence the cohesive energy is calculated too strong.) For NaCl, however, the cohesive energy is with respect to the ions ( $\pm 1e$ ); the  $\text{Na}^+$  and  $\text{Cl}^-$  ions are closed-shell systems and can be computed spin restricted. The atomic spin-polarization energies are as follows (in a.u.): for C,  $-0.0439$ ; for Si,  $-0.0244$ ; for Na,  $-0.0075$ ; for Ni( $d^9s^1$ ),  $-0.0182$ ; for Cu,  $-0.0074$ . The ionic energies with respect to the neutral atoms are (in a.u.) for Na,  $0.1685$ ; for Cl,  $-0.1056$ . The zero-point vibration energies in the crystals are as follows (in a.u./atom): for g-C,  $0.0066$  (Ref. 51); for Si,  $0.0026$  (Ref. 52); for Na,  $0.0005$  (Ref. 53), for Ni,  $0.0015$  (Ref. 53); for Cu,  $0.0015$  (Ref. 53); for NaCl,  $0.0016$  (Ref. 54).

The numerical results are displayed in Table VII. From an overview of the data published by other researchers (Table VII) it transpires that the various DF computations yield significantly different outcomes, with ranges of  $\sim 2\%$  in lattice constants,  $10\%$  in cohesive energies, and up to  $25\%$  in bulk moduli. An obvious first reason for these discrepancies is the use of different DF formulas for the XC interaction. This may (partially) explain the small variation in computed lattice constants. Furthermore, it has been found<sup>9,76</sup> that different DF formulas lead to variations in (total) energies of a few milli-a.u. The differences among the energy data in Table VII are much larger, however. They are hence to be attributed to shape approximations used for the Coulomb potential, unsuitable or ill-converged basis sets, loss of precision by inadequate integration methods in real and/or  $k$  space, and of course to the arbitrariness inherent in pseudopotential approaches. The efforts we have undertaken to control all aspects of precision are therefore fully justified as they appear to be necessary if one wishes to assess the merits and deficiencies of the DF approximation itself.

A comparison of our results with experimental data reveals that the VWN functional leads to an overestimation of the cohesive energy by as much as  $10\text{--}20\%$ , and (ex-

cept for g-C and Si) a too short lattice constant (and a too large bulk modulus). This tendency towards shorter and stronger bonding is also often found in LDF calculations on molecules. The energy fault is (at least partially) due to the *atomic* energies being calculated incorrectly, since multipole splitting is neglected. It has also been argued<sup>77,78</sup> that the discrepancies with experiment should be repaired by incorporating nonlocal terms in the XC functional; gradient exchange corrections have successfully been applied in molecular calculations,<sup>79-82</sup> an efficient setup for their application to periodic systems has been devised,<sup>18</sup> but it has not yet been implemented in our code.

The few Hartree-Fock results that we have found in the literature (see Table VII) severely underestimate the cohesive energies and show once more that correlation plays a crucial role in the understanding of crystals.

Finally we give a summary of computational efforts corresponding to the “default” integration settings ( $A=4$ ,  $K=5$ ). Table VIII displays the number of basis functions using the full LCAO basis sets: basic plus two polarization functions per atom (even where some of the functions may be irrelevant, for Na and NaCl),  $k$  points (in the irreducible BZ), integration points, the maximum number of words stored on disc at any moment during the run, the number of iteration cycles that were used to reach self-consistent-field (SCF) convergence, and the total CPU time (on the Cray Y-MP464), with a percentage distribution of the latter over the three phases of a calculation: preparation (of crystal basis functions mainly), SCF, and properties (“post-SCF”). The data refer in all cases to a single run (i.e., one fixed geometry) with complete SCF convergence.

In calculations on slabs and polymers the relative part of the preparation phase is usually considerably less (typically 40% and 20%, respectively); the relative importance of this part in computations on bulk solids (in particular those with small unit cells) is due to the construction of the crystal basis functions, which gives rise to large sums over lattice points in order to obtain fair precision in the Bloch sums of one-center functions. In systems with very slow SCF convergence with large numbers

TABLE VIII. Data on computational efforts for standard integration settings ( $A=4$ ,  $K=5$ ) with the full LCAO bases. See text.

	g-C	Si	Na	Ni	Cu	NaCl
Basis functions	80	40	18	30	30	38
$k$ points	75	65	35	65	65	65
Integration points ( $10^3$ )	11.6	7.0	5.0	3.4	3.4	7.7
File storage ( $10^6$ words)	155	43	7.9	17	16	45
No. of SCF iterations	20	14	22	46	21	17
Total CPU time (secs)	4287	738	129	689	385	794
Pre-SCF	61%	77%	81%	42%	75%	76%
SCF	39%	23%	19%	58%	27%	24%
Post-SCF	0.1%	0.1%	0.1%	0.1%	0.1%	0.1%

of iterations the SCF part becomes relatively more important.

#### IV. CONCLUSIONS

The analyses of the preceding section demonstrate that all aspects of numerical precision in a calculation are well under control. This applies to the evaluation of integrals in real space and in  $k$  space as well as to the representation of the one-particle wave functions. A straightforward choice of LCAO basis sets with polarization functions leads to rapid and systematic convergence towards the basis-set limit. Plane waves, composite bases, or off-site one-center functions are not required to obtain high precision (at least not for the systems considered in this paper). The relative irrelevance of detailed characteris-

tics of the LCAO basis sets diminishes the need for tedious basis-set optimizations, and hence renders the LCAO method easy to apply with highly precise results, so that the inherent efficiency of this approach, due to the "natural" choice of atomiclike functions, comes to its full right. The calculated properties of bulk g-C, Si, Na, Ni, Cu, and NaCl are supposedly very close to the basis-set limit of the LD (VWN) approximation.

#### ACKNOWLEDGMENTS

The investigation was supported in part by the Netherlands Foundation for Chemical Research (SON) with financial aid from the Netherlands Organization for Scientific Research (ZWO).

\*Electronic address: berttv@sara.nl.

<sup>†</sup>Electronic address: baerends@sara.nl.

<sup>1</sup>D. E. Ellis and G. S. Painter, Phys. Rev. B **2**, 2887 (1970).

<sup>2</sup>J. A. Appelbaum and D. R. Hamann, Phys. Rev. B **8**, 1777 (1973).

<sup>3</sup>O. K. Andersen, Phys. Rev. B **12**, 3060 (1975).

<sup>4</sup>A. Zunger and A. J. Freeman, Phys. Rev. B **15**, 4716 (1977).

<sup>5</sup>D. D. Koelling and G. O. Arbman, J. Phys. F **5**, 2041 (1975).

<sup>6</sup>C. S. Wang and J. Callaway, Comput. Phys. Commun. **14**, 327 (1978).

<sup>7</sup>A. R. Williams, J. Kübler, and C. D. Gelatt, Jr., Phys. Rev. B **19**, 6094 (1979).

<sup>8</sup>E. Wimmer, H. Krakauer, M. Weinert, and A. J. Freeman, Phys. Rev. B **24**, 864 (1981).

<sup>9</sup>M. Weinert, E. Wimmer, and A. J. Freeman, Phys. Rev. B **26**, 4571 (1982).

<sup>10</sup>M. L. Cohen, Phys. Scr. **T1**, 5 (1982).

<sup>11</sup>H. J. F. Jansen and A. J. Freeman, Phys. Rev. B **30**, 561 (1984).

<sup>12</sup>J. W. Davenport, Phys. Rev. B **29**, 2896 (1984).

<sup>13</sup>J. R. Chelikowsky, S. G. Louie, D. Vanderbilt, and C. T. Chain, Int. J. Quantum Chem. Symp. **18**, 105 (1984).

<sup>14</sup>C. B. Haselgrove, Math. Comput. **15**, 323 (1961).

<sup>15</sup>D. E. Ellis, J. Quantum Chem. Symp. **2**, 35 (1968).

<sup>16</sup>P. M. Boerrigter, G. te Velde, and E. J. Baerends, Int. J. Quantum Chem. **33**, 87 (1988).

<sup>17</sup>G. te Velde and E. J. Baerends, J. Comp. Phys. (to be published).

<sup>18</sup>G. te Velde, Ph.D. thesis, Vrije Universiteit Amsterdam, 1990.

<sup>19</sup>R. G. Brown and M. Ciftan, Int. J. Quantum Chem. Symp. **18**, 87 (1984).

<sup>20</sup>R. K. Nesbet, Phys. Rev. B **33**, 8027 (1986).

<sup>21</sup>G. W. Fernando, J. W. Davenport, R. E. Watson, and M. Weinert, Phys. Rev. B **40**, 2757 (1989).

<sup>22</sup>E. J. Baerends, D. E. Ellis, and P. Ros, Chem. Phys. **2**, 41 (1973).

<sup>23</sup>G. Wiesenecker, G. te Velde, and E. J. Baerends, J. Phys. C **21**, 4263 (1988).

<sup>24</sup>G. Wiesenecker and E. J. Baerends, J. Phys. C (to be published).

<sup>25</sup>P. Hohenberg and W. Kohn, Phys. Rev. B **136**, 864 (1964).

<sup>26</sup>W. Kohn and L. J. Sham, Phys. Rev. A **140**, 1133 (1965).

<sup>27</sup>S. H. Vosko, L. Wilk, and M. Nusair, Can. J. Phys. **58**, 1200 (1980).

<sup>28</sup>D. M. Ceperley and B. I. Alder, Phys. Rev. Lett. **45**, 566 (1980).

<sup>29</sup>J. C. Slater, Phys. Rev. **81**, 385 (1951).

<sup>30</sup>F. Herman and S. Skillman, *Atomic Structure Calculations* (Prentice-Hall, Englewood Cliffs, NJ, 1963).

<sup>31</sup>O. Jepsen and O. K. Andersen, Solid State Commun. **9**, 1763 (1971).

<sup>32</sup>G. Lehmann and M. Taut, Phys. Status Solidi B **54**, 469 (1972).

<sup>33</sup>P. Ewald, Ann. Phys. (N.Y.) **64**, 253 (1921).

<sup>34</sup>H. M. Evjen, Phys. Rev. **39**, 675 (1932).

<sup>35</sup>M. P. Tosi, in *Solid State Physics*, edited by F. Seitz and D. Turnbull (Academic, New York, 1964), Vol. 16, p. 1.

<sup>36</sup>M. L. Glasser and I. J. Zucker, in *Theoretical Chemistry: Advances and Perspectives*, edited by D. Henderson (Academic, New York, 1980), Vol. 5, p. 67.

<sup>37</sup>K. Young, J. Math. Phys. **28**, 425 (1987).

<sup>38</sup>B. Sarkar and K. Bhattacharyya, Chem. Phys. Lett. **150**, 419 (1988).

<sup>39</sup>P. W. Atkins, *Physical Chemistry* (Oxford University Press, Oxford, 1987).

<sup>40</sup>G. Arfken, *Mathematical Methods for Physicists* (Academic, New York, 1970).

<sup>41</sup>A. D. Becke, J. Chem. Phys. **76**, 6037 (1982).

<sup>42</sup>A. D. Becke, J. Chem. Phys. **78**, 4787 (1983).

<sup>43</sup>L. Laaksonen, D. Sundholm, and P. Pyykkö, Int. J. Quantum Chem. **27**, 601 (1985).

<sup>44</sup>E. J. Baerends, P. Vernooij, A. Rozendaal, P. M. Boerrigter, M. Krijn, D. Feil, and D. Sundholm, J. Mol. Struct. (Theorchem.) **133**, 147 (1985). The one-electron energies referred to in Table III were an unpublished by-product of this research.

<sup>45</sup>E. Wimmer (private communication).

<sup>46</sup>R. W. Jansen and O. F. Sankey, Phys. Rev. B **36**, 6520 (1987).

<sup>47</sup>R. W. Jansen and B. M. Klein, J. Phys. Condens. Matter **1**, 8359 (1989).

<sup>48</sup>F. D. Murnaghan, Proc. Natl. Acad. Sci. USA **30**, 244 (1944).

<sup>49</sup>P. E. Van Camp, V. E. Van Doren, and J. T. Devreese, Phys. Scr. **35**, 706 (1987).

<sup>50</sup>F. J. Birch, Geophys. Res. **57**, 227 (1952).

<sup>51</sup>J. A. Young and J. K. Koppel, J. Chem. Phys. **42**, 357 (1965).

<sup>52</sup>A. Svane, Phys. Rev. B **35**, 5496 (1987).

<sup>53</sup>V. L. Moruzzi, J. F. Janak, and A. R. Williams, *Calculated Electronic Properties of Metals* (Pergamon, New York, 1978).

<sup>54</sup>Zahlenwerte und Funktionen aus Physik, Chemie, Astronomie,

- Geophysik und Technik*, Landolt-Börnstein (Springer, Berlin, 1955).
- <sup>55</sup>C. Kittel, *Introduction to Solid State Physics* (Wiley, New York, 1976).
- <sup>56</sup>M. T. Yin and M. L. Cohen, Phys. Rev. B **26**, 5668 (1982).
- <sup>57</sup>A. Svane and O. K. Andersen, Phys. Rev. B **34**, 5512 (1986).
- <sup>58</sup>W. R. L. Lambrecht and O. K. Andersen, Phys. Rev. B **34**, 2439 (1986).
- <sup>59</sup>H. J. F. Jansen and A. J. Freeman, Phys. Rev. B **33**, 8629 (1986).
- <sup>60</sup>K. J. Chang and M. L. Cohen, Phys. Rev. B **35**, 8196 (1987).
- <sup>61</sup>A. Oshiyama and M. Saito, J. Phys. Soc. Jpn. **56**, 2104 (1987).
- <sup>62</sup>M. H. Kang, R. C. Tater, E. J. Mele, and P. Soven, Phys. Rev. B **35**, 5457 (1987).
- <sup>63</sup>K. Terakura, T. Oguchi, T. Mohri, and K. Watanabe, Phys. Rev. B **35**, 2169 (1987).
- <sup>64</sup>M. Farjam and H. B. Shore, Phys. Rev. B **37**, 1059 (1988).
- <sup>65</sup>J. R. Chelikowsky and M. Y. Chou, Phys. Rev. B **38**, 7966 (1988).
- <sup>66</sup>Z. W. Lu, S.-H. Wei, and A. Zunger, Phys. Rev. B **41**, 2669 (1990).
- <sup>67</sup>A. M. Rappe, K. M. Rabe, E. Kaxiras, and J. D. Joannopoulos, Phys. Rev. B **41**, 1227 (1990).
- <sup>68</sup>G. E. Bacon, Acta Crystallogr. **4**, 558 (1951).
- <sup>69</sup>A. Zunger, Phys. Rev. B **17**, 626 (1978).
- <sup>70</sup>H. J. F. Jansen and A. J. Freeman, Phys. Rev. B **35**, 8207 (1987).
- <sup>71</sup>A. Von Ludsteck, Acta Crystallogr. A **28**, 59 (1972).
- <sup>72</sup>W. B. Gauster and J. J. Fritz, J. Appl. Phys. **45**, 3309 (1974).
- <sup>73</sup>O. K. Andersen, J. Madsen, U. K. Poulsen, O. Jepsen, and J. Kollár, Physica B **86-88**, 249 (1977).
- <sup>74</sup>K. A. Gschneidner, in *Solid State Physics*, edited by F. Seitz and D. Turnbull (Academic, New York, 1964), Vol. 16, p. 295.
- <sup>75</sup>Y. Baskin and L. Mayer, Phys. Rev. **100**, 544 (1955).
- <sup>76</sup>H. J. F. Jansen and S. S. Peng, Phys. Rev. B **37**, 2689 (1988).
- <sup>77</sup>A. D. Becke, J. Chem. Phys. **84**, 4524 (1986).
- <sup>78</sup>A. D. Becke, Phys. Rev. A **38**, 3098 (1988).
- <sup>79</sup>T. Ziegler, V. Tschinke, and A. D. Becke, Polyhedron **6**, 685 (1987).
- <sup>80</sup>T. Ziegler, V. Tschinke, and A. D. Becke, J. Am. Chem. Soc. **109**, 1351 (1987).
- <sup>81</sup>T. Ziegler, V. Tschinke, and C. Ursenbach, J. Am. Chem. Soc. **109**, 4825 (1987).
- <sup>82</sup>T. Ziegler, V. Tschinke, L. Versluis, and E. J. Baerends, Polyhedron **7**, 1625 (1988).